Research Article | Vol. 30, No. 14 / 4 Jul 2022 / Optics Express 24924
Optics EXPRESS

Technologically feasible quasi-edge states and topological Bloch oscillation in the synthetic space

XIAOXIONG WU,[1] LUOJIA WANG,[1] GUANGZHEN LI,[1] DALI CHENG,[1,2] DANYING YU,[1] YUANLIN ZHENG,[1] VLADISLAV V. YAKOVLEV,[3] LUQI YUAN,[1,*] AND XIANFENG CHEN[1,4,5,6]

[1]*State Key Laboratory of Advanced Optical Communication Systems and Networks, School of Physics and Astronomy, Shanghai Jiao Tong University, Shanghai 200240, China*
[2]*Ginzton Laboratory and Department of Electrical Engineering, Stanford University, Stanford, CA 94305, USA*
[3]*Texas A&M University, College Station, TX 77843, USA*
[4]*Shanghai Research Center for Quantum Sciences, Shanghai 201315, China*
[5]*Jinan Institute of Quantum Technology, Jinan 250101, China*
[6]*Collaborative Innovation Center of Light Manipulation and Applications, Shandong Normal University, Jinan 250358, China*
[*]*yuanluqi@sjtu.edu.cn*

Abstract: The dimensionality of a physical system is one of the major parameters defining its physical properties. The recently introduced concept of synthetic dimension has made it possible to arbitrarily manipulate the system of interest and harness light propagation in different ways. It also facilitates the transformative architecture of system-on-a-chip devices enabling far reaching applications such as optical isolation. In this report, a novel architecture based on dynamically-modulated waveguide arrays with the Su-Schrieffer-Heeger configuration in the spatial dimension is proposed and investigated with an eye on a practical implementation. The propagation of light through the one-dimensional waveguide arrays mimics time evolution of the field in a synthetic two-dimensional lattice. The addition of the effective gauge potential leads to an exotic topologically protected one-way transmission along adjacent boundary. A cosine-shape isolated band, which supports the topological Bloch oscillation in the frequency dimension under the effective constant force, appears and is localized at the spatial boundary being robust against small perturbations. This work paves the way to improved light transmission capabilities under topological protections in both spatial and spectral regimes and provides a novel platform based on a technologically feasible lithium niobate platform for optical computing and communication.

1. Introduction

The introduction of a notion of synthetic dimension has made it possible to explore and practically realize higher-dimensional concepts in lower-dimensional devices. This way, on-chip devices with reduced complexity and improved and expanded functionalities become technologically feasible. In photonics, synthetic dimension shows its flexible capability for constructing artificial lattices with exotic connectivities [1–3] by connecting discrete optical modes along different degrees of freedom of light, such as frequency [4,5], orbital angular momentum [6], and temporal pulse information [7]. This unique opportunity therefore triggers extensive interests in exploring optical architectures that are hard to be practically implemented in real space [8–11] in order to explore exciting optical phenomena such as those associated with Bloch oscillation [12–15], topological quantum matter [16–19], non-Hermitian Hamiltonian [20–23], and higher-order

#462156 https://doi.org/10.1364/OE.462156
Journal © 2022 Received 27 Apr 2022; revised 15 Jun 2022; accepted 15 Jun 2022; published 24 Jun 2022

Optics EXPRESS

topological physics [24,25]. Among different approaches, the design of synthetic dimension, which includes the frequency axis of light, provides an intriguing opportunity for manipulating light properties along both spatial and spectral axes in a manner under the topological protection [1–3]. This is highly desirable for potential applications in optical communications and optical computing. In doing so, optical modes at different frequencies are utilized and connected through external modulations, so that energy at each optical mode can hop to nearby modes to construct an effective tight-binding model along the optical frequency axis. In particular, such tight-binding lattices, which can be extended into higher-dimensional space including the synthetic frequency dimension, have been shown in a system of dynamically-modulated ring resonators [11]. While there are several ongoing efforts in advancing frontiers of synthetic frequency dimension in on-chip rings [26,27], the fabrication process of large-scale devices based on those physical principles remains to be technologically challenging.

Photonic waveguide undergoing fast electro-optic modulation shows a promising platform in creating synthetic frequency dimension [28]. In this case, the light propagation inside the waveguide follows a Schrödinger-like equation where the propagation distance of light mimics the time evolution of the physical system [29]. A proper space-time modulation by external electric signals on the waveguide can connect different frequency components of the propagating light and therefore creates a one-dimensional synthetic frequency dimension, as shown in Fig. 1(a) [28]. Such platform holds important possibility in manipulating the spectral information of light in the on-chip devices, thanks to the recent developments of state-of-art technologies in lithium niobate-on-insulator (LNOI) [30–37]. However, the study of extensions beyond one dimension in coupled waveguides under modulations is still missing to the best of our knowledge. The key issue here is the potential crosstalk of the applied modulation signals, i.e., the applied external control signals on two nearby modulated waveguides may interfere each other. A natural way to get around this issue is to arrange coupled waveguides with spaced modulations (i.e., only waveguides marked as A are modulated) [see Fig. 1(b)]. Hence, it is highly desired for a detailed theoretical understanding of such design in constructing synthetic space beyond one dimension and then explore the corresponding exciting physics.

In this report, we investigate physical phenomena in one-dimensional weakly coupled waveguide arrays, where electro-optic modulated waveguides and unmodulated waveguides are arranged alternatively as shown in Fig. 1(b). Such a system can minimize the direct crosstalk of modulation signals in-between two modulated waveguides, and hence supports a two-dimensional synthetic lattice for the travelling light along waveguides, whose dimensions are spatial and frequency ones [see Fig. 1(c)]. We choose spatial couplings between waveguides following the Su-Schrieffer-Heeger (SSH) configuration, while introducing the effective magnetic flux by adding non-uniform modulation phases in each modulated waveguide. Our results show that this hybrid system supports exotic topological edge states (*quasi-edge state*s), where the wavepacket of light evolving unidirectionally along the frequency dimension is not localized at the edge. Another important prediction is that the topological Bloch oscillation is readily seen in simulations, where the oscillation of frequency modes is located at the boundary of waveguide arrays and is robust against small disorders. Thus, this work not only shows important topological photonic phenomena in a hybrid synthetic lattice, but also paves potential ways to manipulate the frequency of light under topological protection in modulated waveguide arrays. Moreover, our study could bring possible applications involving harnessing light in optical communications with the integrated photonics.

Optics EXPRESS

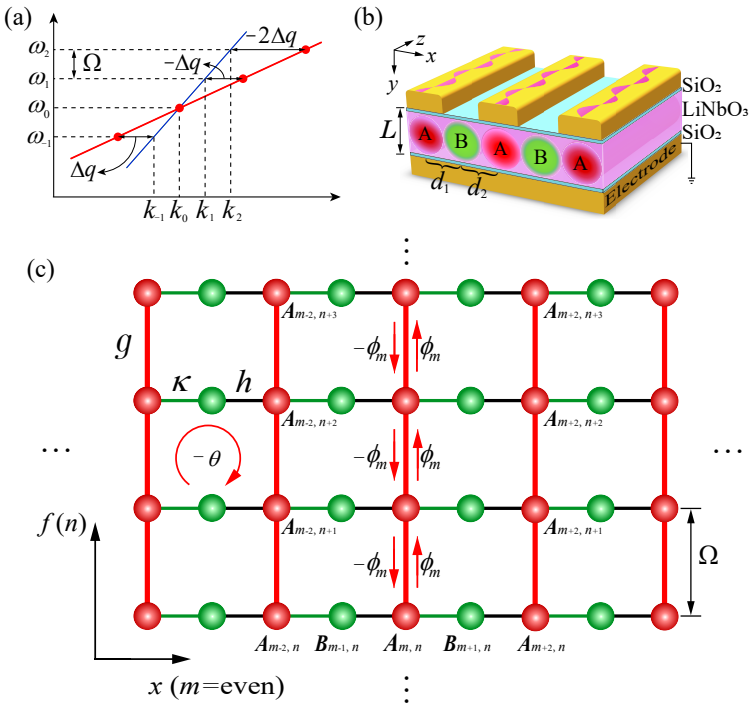

Fig. 1. The illustration of synthetic frequency dimension in modulated waveguide arrays (a) Discrete frequency modes of the light (red dots) are connected by the travelling-wave dynamic modulation (marked as red line). Blue line gives the intrinsic dispersion curve $[\omega = k(\partial\omega/\partial k)]$ of each waveguide where $\Delta q = q - Q$ denotes the wavevector mismatching for optical modes at frequencies ω_n propagating inside waveguides. Here, Q is the modulation wavevector, and $q \equiv \Omega(\partial k/\partial\omega)$ denotes the phase-matching wavevector. (b) The schematic of waveguide arrays based on LNOI technology, where waveguides labeled as A and B alternatively arranged in-between SiO_2 buffering layers and only waveguides of type A are modulated by external voltages. Note that the colors of A (in red) and B (in green) denote the optical mode distributions inside waveguides. (c) Constructed two-dimensional synthetic lattice from (b).

2. Model and theory

We start from studying a realistic experimental platform based on LNOI as shown in Fig. 1(b). One-dimensional waveguide arrays are proposed to be fabricated in micrometer-thick LNOI using proton-exchange or titanium in-diffusion method [38,39], as well as in lithium niobate thin films using shallow-etched or loaded waveguide array structure [40–42]. Alternative platforms include nano-waveguide arrays [18]. Such designed structure supports two types of waveguides (labelled by A and B respectively) weakly coupled between each other. We propose that waveguides of type A are undergoing dynamic modulations by covering positive and ground electrodes while waveguides of type B experience no modulation. The upper and lower buffering layers of SiO_2 (typically 2 micrometers) are introduced to reduce metallic loss from the electrodes. The bottom metal layer serves as the ground electrode. Therefore, there is no significant crosstalk of the applied electric fields between two modulated waveguides. The distance between waveguide centers of types A and B can be larger than 5 micrometers due to a weak transverse light confinement, which makes the fabrication of electrodes feasible in experiments.

Optics EXPRESS

Near the reference frequency ω_0, we assume linear dispersion $\omega = k\,(\partial\omega/\partial k)$. A sinusoidal travelling-wave radio frequency modulation is applied inside each waveguide of type A, i.e., $\cos(\Omega t - Qz + \phi)$, where Ω is the modulation frequency, z is the propagation direction, ϕ is the modulation phase, and $Q \approx q \equiv \Omega\,(\partial k/\partial\omega)$ is the modulation wavevector [13,28,43,44]. Hence discrete modes in waveguides arrays can be excited at frequencies $\omega_n = \omega_0 + n\Omega$ [see Fig. 1(a)], with the effective modulation strength between adjacent modes g and wavevector mismatching $\Delta q = q - Q$, with $|\Delta q| << Q$. Here, Fig. 1(a) provides illustrative curves of the intrinsic waveguide dispersion and travelling-wave dynamic modulation, where the latter one can be further controlled [28,45]. Note that $\Delta q = 0$ or $Q/\Omega = \partial k/\partial\omega$ gives the phase-matching condition [28]. There is no direct modulation applied inside waveguides of the type B. The propagating modes at frequencies ω_n in the m^{th} waveguide of type A and the $(m{+}1)^{\text{th}}$ waveguide of type B therefore construct a synthetic two-dimensional space labelled by $A_{m,n}$ and $B_{m+1,n}$ respectively as illustrated in Fig. 1(c) where we set m as an even integer. We further consider a non-uniform distribution of waveguides in the x direction, i.e., we set the distance between centers of the m^{th} waveguide of type A with the $(m{+}1)^{\text{th}}$ waveguide of type B as d_1 and the distance between centers of the $(m{-}1)^{\text{th}}$ waveguide of type B with the m^{th} waveguide of type A as d_2. Slightly difference between d_1 with d_2 can bring non-uniform couplings between modes at the same frequency ω_n in nearby waveguides, where coupling strengths κ between $A_{m,n}$ and $B_{m+1,n}$, h between $B_{m-1,n}$ and $A_{m,n}$ can be different.

We now consider the phase-matching modulation with $\Delta q = 0$, while the consideration of $\Delta q \neq 0$ is discussed in Section 3.3. By comparing the wave equation describing the light travelling in waveguides and the Schrödinger equation [13,28,29,46], the effective Hamiltonian gives

$$H = \sum_{m=\text{even},n} \left(\kappa a^{\dagger}_{m,n} b_{m+1,n} + h b^{\dagger}_{m-1,n} a_{m,n} + g a^{\dagger}_{m,n} a_{m,n+1} e^{-i\phi_m}\right) + h.c., \tag{1}$$

where $a_{m,n}$ and $b_{m+1,n}$ ($a^{\dagger}_{m,n}$ and $b^{\dagger}_{m+1,n}$) are annihilation (creation) operators for modes $A_{m,n}$ and $B_{m+1,n}$, respectively. We assume modulations in every two nearby waveguides of type A are different by a constant phase θ, by applying same travelling-wave signal shapes with a constant pulse delay on each electrode. Therefore, the corresponding modulation phase on the m^{th} waveguide of type A gives $\phi_m = m\theta/2$, as shown in Fig. 1(c). The constructed synthetic two-dimensional lattice hence provides a set of standard one-dimensional SSH lattices [47–51] in the spatial dimension, connected along the synthetic frequency dimension. Moreover, the introduced distribution of modulation phases in system creates the effective gauge potential $|\mathbf{A}_{\text{eff}}| \propto \theta$ in the synthetic lattice [52].

3. Results

3.1. Band structures of the model

We first consider a uniform distribution of waveguide arrays $h = \kappa$ and $\kappa = g$ to give a simple example of understanding our model. For infinite modes in both x and f axes, θ chosen as $(2\pi/\theta)$ being an integer, the synthetic lattice holds the translational symmetry with the periodicity of Ω in the f direction and the periodicity of $(2\pi/\theta) \times (d_1 + d_2)$ in the x direction. We plot the projected band structure of our system, ε, in Fig. 2(a), which shows Hofstandter butterfly-like spectrum. Due to additional lattice sites on waveguides of type B in each plaquette, the spectrum exhibits double amounts of open gaps, compared to the standard Hofstandter butterfly spectrum [53–55]. In Fig. 2(b), we plot the band structure for the case of $\theta = \pi/2$ with open boundary in the x direction but still assuming infinite sites along the frequency dimension. This makes k_f, which is reciprocal to the f axis, being a good quantum number. We choose 41 waveguides of type A and 40 waveguides of type B, i.e., $m \in [-40, 40]$, where even (odd) integers refer to the waveguide of type A (B). One sees there are 4 pairs of edge states inside 4 gaps, which are

Optics EXPRESS

double compared to the energy diagram in the conventional rectangular lattice [4,5,52,56]. The duplicity of edge states is understandable due to pairs of sites (A and B) on boundaries along the x axis. Here we note that the energy of the band structure, ε, refers to the shift of wavevector for a probe signal propagating in the z direction [57].

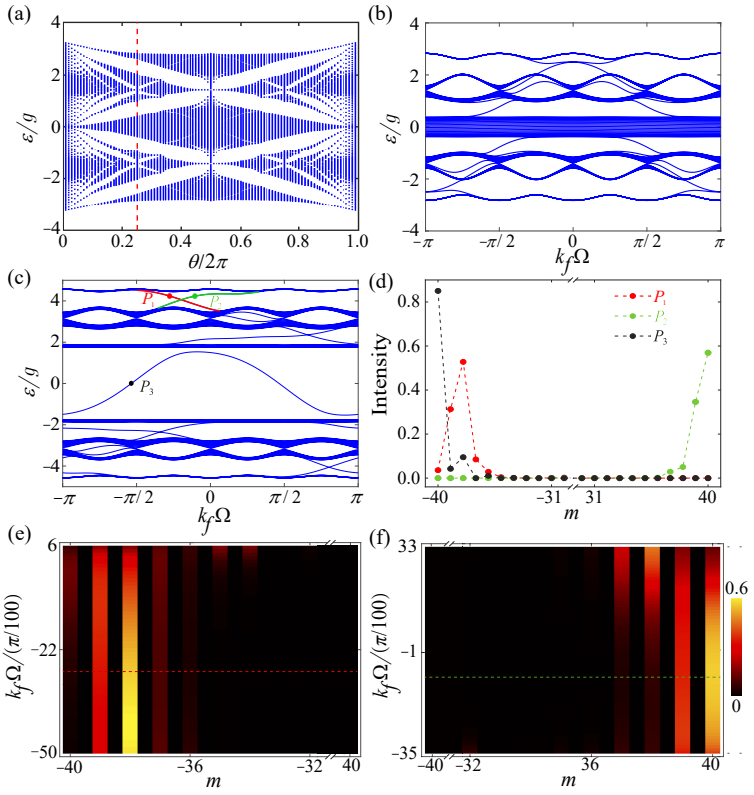

Fig. 2. Band analysis showing topological (quasi-)edge states and isolated band. (a) The projected band structure of infinite synthetic lattice versus θ for $h = \kappa = g$. (b) The projected band structure with finite waveguide arrays ($m \in [-40, 40]$) versus k_f for $\theta = \pi/2$, which is labelled by the red dashed line in (a). (c) The projected band structure with finite waveguide arrays ($m \in [-40, 40]$), where $h = 3g$, $\kappa = g$, and $\theta = \pi/2$. (d) Distributions of field intensities for states at P_1 (red), P_2 (green), and P_3 (black) labelled in (c), respectively. (e) and (f) Normalized intensity distributions of topological edge states versus k_f labelled by red and green lines in (c), respectively.

We next explore configurations of $h \neq \kappa$, corresponding to connected SSH lattices under the effective magnetic flux. Such a model combines two different topological features, which brings interesting results that we will discuss in the rest of our paper. As an example, we study the case of $h = 3g$ while $\kappa = g$, and calculate the band structure [see Fig. 2(c)] with other parameters being the same as those in Fig. 2(b). Similarly, there are four pairs of edge states in gaps. However, the striking feature is that the middle bulk band near $\varepsilon = 0$ is open and an isolated band exists. This isolated band corresponds to the topological boundary state in the one-dimensional SSH lattice, but shows a cosine-like band shape, meaning the connection of such boundary states along the additional frequency dimension. In Fig. 2(d), we plot the distribution of field intensities of the isolated band indicated by the black dot in Fig. 2(c), where the energy of field is located at the left boundary and decays into the bulk. On the other hand, field intensity distributions of pairs

Optics EXPRESS

of edge states in the top band gap labelled by red and green dots are also plotted. While for one edge state (green dot), the field is localized at the right boundary, the other state (red dot) exhibits a unusual feature that the field is focused on the third waveguide (the second waveguide of type A) from the left and decays exponentially into two sides, which we refer it as quasi-edge state throughout this paper. This quasi-edge state is a unique consequence from the combination of both the effective magnetic flux and the non-trivial connectivity from SSH configuration, which is fundamentally different from the edge states in the conventional two-dimensional square lattice under the magnetic flux [4,5,52,56]. We further plot normalized intensity distributions of edge states (red and green lines) versus k_f, which corresponds to edge states in-between band gap in the k_f-space, as shown in Figs. 2(e) and 2(f), respectively. One notes that intensity distributions in Fig. 2(f) show conventional characteristics of the edge state, where energy of light is localized on the right boundary when it is near the middle of the gap $k_f \sim -0.19\pi/\Omega$. However, in Fig. 2(e), one sees that, in the majority of the gap with $k_f \in (-0.5\pi, 0.06\pi)/\Omega$, the corresponding distributions of light exhibit the maximum peak in the third waveguide from the left, indicating the quasi-edge state exhibits along nearly the entire edge band in-between the band gap, which results from the competition between two topological effects, namely the quantum Hall effect and the SSH effect.

3.2. Topological quasi-edge states

To explore dynamics associated with edge states in the synthetic lattice, we simulate the wave propagation under the Hamiltonian Eq. (1) by assuming the wave function as

$$|\varphi(z)\rangle = \sum_{m=\text{even},n} \left(v_{a,m,n} a^{\dagger}_{m,n} + v_{b,m+1,n} b^{\dagger}_{m+1,n} \right) |0\rangle , \tag{2}$$

where $v_{a,m,n}$, $v_{b,m+1,n}$ being amplitudes of light at modes $A_{m,n}$ and $B_{m+1,n}$, respectively. Using the Schrödinger-like equation, $i\frac{\mathrm{d}}{\mathrm{d}z}|\varphi(z)\rangle = H\,|\varphi(z)\rangle$, we obtain coupled-mode equations

$$\begin{aligned} i\mathrm{d}v_{a,m,n}/\mathrm{d}z &= \kappa v_{b,m+1,n} + h v_{b,m-1,n} + g(v_{a,m,n-1}e^{-i\phi_m} + v_{a,m,n+1}e^{i\phi_m}) + is\delta_{m,M}\delta_{n,0}, \\ i\mathrm{d}v_{b,m+1,n}/\mathrm{d}z &= \kappa v_{a,m,n} + h v_{a,m+2,n} \qquad (m = \text{even}). \end{aligned} \tag{3}$$

Here we choose the exciting source $s = e^{i\Delta k z}$ where Δk stands for the wavevector mismatching of the input light from the reference mode $k_0 = \omega_0/(\partial\omega/\partial k)$. Note that Δk is the same momentum mismatching as ε in the band structure, so by choosing Δk in the source, one can selectively excite the state on the band structure. In Eq. (3), the source term including s is added following the temporal input-output formalism [58,59], describing the external excitation of the system. In potential experiments, such source is injected into waveguide arrays from adding an auxiliary waveguide (on the side or beneath waveguide arrays) [60–62], very weakly coupled to the M^{th} waveguide with the loss from coupling between the auxiliary waveguide and waveguide arrays being negligible. To better illustrate the topological protection, we set the artificial boundary at the frequency dimension and assume $n \in [-40, 40]$, which can be realized by carefully engineering the dispersion curve of the waveguide [4,63]. However, such artificial boundary is not mandatory to be designed in order to observe exotic quasi-edge states in the synthetic lattice.

We perform simulations corresponding to the (quasi-)edge state by selectively exciting the leftmost waveguide and the rightmost waveguide respectively at $\Delta k = 4.237g$ near the 0^{th} frequency mode. We assume the length of waveguide arrays being $z = 50g^{-1}$. The simulations are performed by numerically solving differential Eq. (3) with discretizing the spatial dimension z. Figures 3(a) and 3(b) show simulation results of the normalized field distribution for the 81×81 synthetic lattice of different waveguides and frequency modes, that are collected on the other side of waveguide arrays. One sees topologically-protected one-way propagating modes in both

Optics EXPRESS

cases, where the field gets turned at the corner and transports in the synthetic two-dimensional space unidirectionally without back-reflection. Moreover, as indicated by band structure analysis, we find quasi-edge state near the left boundary of the synthetic lattice, where the third waveguide from the left is excited for the most. For the external excitation on the leftmost waveguide, the energy of light tunnels into the -38^{th} waveguide quickly and then gets most frequency down conversion inside the -38^{th} waveguide mostly, while for the excitation on the right, the light transports to the -38^{th} waveguide after it circulates counter-clock-wisely through the top boundary. Exotic one-way edge state therefore exhibits where the first two waveguides from the left are very weakly excited in both cases.

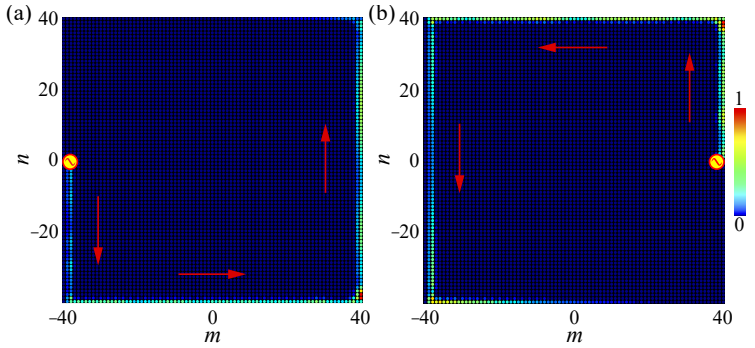

Fig. 3. Topologically-protected one-way (quasi-)edge states. (a) and (b) Simulation results at $z = 50g^{-1}$ in the synthetic space with an external source $s = e^{i\Delta kz}$ and $\Delta k = 4.237g$ excited at the leftmost and rightmost waveguides, respectively.

3.3. *Topological Bloch oscillation*

Previously we showed the isolated band near $\varepsilon = 0$ in Fig. 2(c). Larger $h = 5g$ can increase the middle gap and the isolated band gives a cleaner cosine-shape as shown in Fig. 4(a). In Fig. 4(b), we plot normalized intensity distributions of the isolated band in the entire range of the first Brillouin zone, i.e., $k_f \in [-\pi/\Omega, \pi/\Omega]$. We can see that the field mostly distributes on the left boundary due to the SSH configuration in our designed model.

Now we consider the wavevector mismatching case with $\Delta q \neq 0$ [13], which leads to the Hamiltonian:

$$\tilde{H} = \sum_{m=\text{even},n} \left[\kappa a^{\dagger}_{m,n} b_{m+1,n} + h b^{\dagger}_{m-1,n} a_{m,n} + g a^{\dagger}_{m,n-1} a_{m,n} e^{-i(\Delta q z + \phi_m)}\right] + h.c., \tag{4}$$

implying a constant effective force $F = -\Delta q$ [12,14,15,64]. Similar effective force in a one-dimensional photonic lattice can lead to Bloch oscillation of light [12–15,47,64]. Here, we find that the isolated band provides a unique topological platform to explore the Bloch oscillation under the effective force.

As demonstrations in simulations, we choose a Gaussian-shape pulse as the excitation source, which reads as $s(z) = e^{-8\ln 2(gz-1)^2}$, and excite the 0^{th} mode in the leftmost waveguide. In Fig. 4(c), we show the evolution of the field distributed on frequency modes inside the leftmost waveguide. The Bloch oscillation feature in the frequency dimension with the spatial periodicity about $Z_B = 2\pi/|\Delta q| \approx 12.6g^{-1}$ can be seen. We further define the ratio of energy distribution on the leftmost waveguide $I_l = \sum_n |v_{a,-40,n}|^2 / \sum_{m=\text{even},n} \left(|v_{a,m,n}|^2 + |v_{b,m+1,n}|^2\right)$, and plot I_l versus the propagation distance z in Fig. 4(d) [see the red curve]. One sees that I_l slightly drops from 1 and then quickly stabilizes near 93% throughout the entire propagation in waveguide arrays. The

Optics EXPRESS

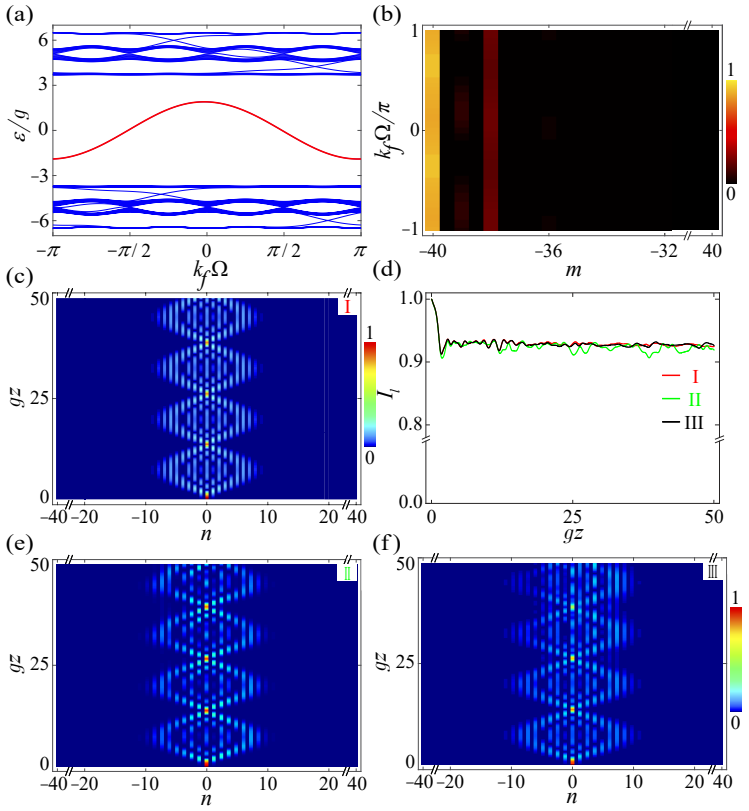

Fig. 4. Spectral Bloch oscillation localized in the leftmost waveguide under topological protection. (a) The projected band structure with finite waveguide arrays ($m \in [-40, 40]$), where $h = 5g$, $\kappa = g$, and $\theta = \pi/2$, where middle isolated band is labelled in red. (b) Normalized intensity distributions of isolated band versus k_f labelled by the red curve in (a) in the first Brillouin zone. (c) The evolution of the field propagating along the z direction distributed on the n^{th} frequency modes inside the leftmost waveguide. (d) The ratios of energy distributions on the leftmost waveguide I_l versus the propagation distance z. The red (I), green (II) and black (III) curves correspond to simulation results in (c), (e), (f), correspondingly. (e) and (f) The evolutions of the field propagating along the z direction distributed on the n^{th} frequency modes inside the leftmost waveguide with the disorders of h, κ, g and disorders of Δq, respectively, included in simulations.

Optics EXPRESS

energy of light is mainly localized at the leftmost waveguide during the evolution of the Bloch oscillation, indicating the intensity distribution of isolated band that exhibits the localization on the left boundary (the leftmost waveguide).

To further demonstrate the topological protection of the Bloch oscillations shown in this configuration of our model, we add disorders into the system and perform simulations. In details, we first consider disorders in coupling strengths (κ and h) and modulation amplitude (g), where a coefficient $(1 + R \cdot \delta_1)$ is multiplied on each κ, h, and g, respectively. Here R is the random number generated in-between $(-0.5, 0.5)$, and δ_1 is a constant for labelling the amplitude of disorders. In Fig. 4(e), we plot the evolution of the field distributed on frequency modes inside the leftmost waveguide with $\delta_1 = 0.2$. One can see the pattern of the Bloch oscillation still preserves. More importantly, as indicated by the green curve in Fig. 4(d), I_l remains >90% throughout the entire z in the simulation, showing the topological protection of the localization feature of the isolated band near $\varepsilon = 0$. We also include disorders in the effective force, with similarly a multiplication of $(1 + R \cdot \delta_2)$ onto each Δq in Eq. (4). In the case of $\delta_2 = 0.025$, we find there exists the pattern of the Bloch oscillation in the simulation, as shown in Fig. 4(f), while I_l [in black curve in Fig. 4(d)] is larger than 90% throughout the propagation in waveguide arrays. Although we note that if further larger δ_2 is used, the effective force is destroyed and pattern of the Bloch oscillation is gradually distorted, the energy of light is still localized at the leftmost waveguide. In both cases, we find the robustness against small disorders while the evolution of the Bloch oscillation inside the leftmost waveguide in our proposed system.

4. Conclusion

In summary, we propose and meticulously investigate a novel synthetic-dimension device architecture based on LNOI waveguide arrays arranged in the SSH configuration. Such a device, being exposed to spaced-distributed dynamic modulations, aims at extending synthetic space beyond one dimension in modulated waveguides. The proposed architecture can avoid the direct crosstalk of modulation signals and then support a two-dimensional lattice under the effective gauge field in a synthetic space including spatial and frequency dimensions. The combination of the effective magnetic field and the SSH configuration brings quasi-edge state, where the topological one-way mode supports the peak intensity distribution in the the third waveguide from the left boundary. A cosine-shape isolated band structure has been explored, and the resulting Bloch oscillation along the frequency dimension under an effective force has been found to be localized at the spatial boundary and robust against small disorders. The proposed model is highly relevant to the current start-of-the-art LNOI technology, and therefore could be used for further experimental advancements leading to systems with on-chip applications. Further studies can be focused onto the study of non-Hermitian gain-loss modulations on waveguide arrays, which maybe experimental challenging, however, can bring further interest in such structures [65,66]. Although this model is explored in the modulated waveguide array system, it can also be potentially implemented in other platforms such as static waveguide arrays [16,29,67], ring resonators [11], dynamically reconfigurable photonic crystals [53,68], time-multiplexed network [69,70], and cold atoms [71,72], showing very rich opportunities for studying interesting topological phenomena in both real space and synthetic space.

Funding. National Natural Science Foundation of China (11974245, 12104297, 12122407); National Key Research and Development Program of China (2017YFA0303701); Shanghai Municipal Science and Technology Major Project (2019SHZDZX01); Natural Science Foundation of Shanghai (19ZR1475700); National Science Foundation (CMMI-1826078); Air Force Office of Scientific Research (FA9550-15-1-0517, FA9550-20-1-0366); National Institutes of Health (1R01GM127696-01, 1R21GM142107-01); Cancer Prevention and Research Institute of Texas (RP180588).

Acknowledgments. L.Y. thanks the sponsorship from Yangyang Development Fund and the support from the Program for Professor of Special Appointment (Eastern Scholar) at Shanghai Institutions of Higher Learning. X.C. also acknowledges the support from Shandong Quancheng Scholarship (00242019024).

Optics EXPRESS

Disclosures. The authors declare no conflicts of interest.

Data availability. Data underlying the results presented in this paper are not publicly available at this time but may be obtained from the authors upon reasonable request.

References

1. L. Yuan, Q. Lin, M. Xiao, and S. Fan, "Synthetic dimension in photonics," Optica **5**(11), 1396–1405 (2018).
2. T. Ozawa and H. M. Price, "Topological quantum matter in synthetic dimensions," Nat. Rev. Phys. **1**(5), 349–357 (2019).
3. E. Lustig and M. Segev, "Topological photonics in synthetic dimensions," Adv. Opt. Photonics **13**(2), 426–461 (2021).
4. L. Yuan, Y. Shi, and S. Fan, "Photonic gauge potential in a system with a synthetic frequency dimension," Opt. Lett. **41**(4), 741–744 (2016).
5. T. Ozawa, H. M. Price, N. Goldman, O. Zilberberg, and I. Carusotto, "Synthetic dimensions in integrated photonics: From optical isolation to four-dimensional quantum Hall physics," Phys. Rev. A **93**(4), 043827 (2016).
6. X.-W. Luo, X. Zhou, C.-F. Li, J.-S. Xu, G.-C. Guo, and Z.-W. Zhou, "Quantum simulation of 2D topological physics in a 1D array of optical cavities," Nat. Commun. **6**(1), 7704 (2015).
7. A. Regensburger, C. Bersch, M.-A. Miri, G. Onishchukov, D. N. Christodoulides, and U. Peschel, "Parity-time synthetic photonic lattices," Nature **488**(7410), 167–171 (2012).
8. D. Jukić and H. Buljan, "Four-dimensional photonic lattices and discrete tesseract solitons," Phys. Rev. A **87**(1), 013814 (2013).
9. A. Schwartz and B. Fischer, "Laser mode hyper-combs," Opt. Express **21**(5), 6196–6204 (2013).
10. B. A. Bell, K. Wang, A. S. Solntsev, D. N. Neshev, A. A. Sukhorukov, and B. J. Eggleton, "Spectral photonic lattices with complex long-range coupling," Optica **4**(11), 1433–1436 (2017).
11. L. Yuan, A. Dutt, and S. Fan, "Synthetic frequency dimensions in dynamically modulated ring," APL Photonics **6**(7), 071102 (2021).
12. L. Yuan and S. Fan, "Bloch oscillation and unidirectional translation of frequency in a dynamically modulated ring resonator," Optica **3**(9), 1014–1018 (2016).
13. C. Qin, L. Yuan, B. Wang, S. Fan, and P. Lu, "Effective electric-field force for a photon in a synthetic frequency lattice created in a waveguide modulator," Phys. Rev. A **97**(6), 063838 (2018).
14. G. Li, Y. Zheng, A. Dutt, D. Yu, Q. Shan, S. Liu, L. Yuan, S. Fan, and X. Chen, "Dynamic band structure measurement in the synthetic space," Sci. Adv. **7**(2), eabe4335 (2021).
15. H. Chen, N. Yang, C. Qin, W. Li, B. Wang, T. Han, C. Zhang, W. Liu, K. Wang, H. Long, X. Zhang, and P. Lu, "Real-time observation of frequency Bloch oscillations with fibre loop modulation," Light: Sci. Appl. **10**(1), 48 (2021).
16. E. Lustig, S. Weimann, Y. Plotnik, Y. Lumer, M. A. Bandres, A. Szameit, and M. Segev, "Photonic topological insulator in synthetic dimensions," Nature **567**(7748), 356–360 (2019).
17. A. Dutt, Q. Lin, L. Yuan, M. Minkov, M. Xiao, and S. Fan, "A single photonic cavity with two independent physical synthetic dimensions," Science **367**(6473), 59–64 (2020).
18. Z.-W. Yan, Q. Wang, M. Xiao, Y.-L. Zhao, S.-N. Zhu, and H. Liu, "Probing rotated Weyl physics on nonlinear lithium niobate-on-insulator chips," Phys. Rev. Lett. **127**(1), 013901 (2021).
19. D. Yu, B. Peng, X. Chen, X.-J. Liu, and L. Yuan, "Topological holographic quench dynamics in a synthetic frequency dimension," Light: Sci. Appl. **10**(1), 209 (2021).
20. S. Weidemann, M. Kremer, T. Helbig, T. Hofmann, A. Stegmaier, M. Greiter, R. Thomale, and A. Szameit, "Topological funneling of light," Science **368**(6488), 311–314 (2020).
21. Y. Song, W. Liu, L. Zheng, Y. Zhang, B. Wang, and P. Lu, "Two-dimensional non-Hermitian skin effect in a synthetic photonic lattice," Phys. Rev. Appl. **14**(6), 064076 (2020).
22. K. Wang, A. Dutt, K. Y. Yang, C. C. Wojcik, J. Vučković, and S. Fan, "Generating arbitrary topological windings of a non-Hermitian band," Science **371**(6535), 1240–1245 (2021).
23. K. Wang, A. Dutt, C. C. Wojcik, and S. Fan, "Topological complex-energy braiding of non-Hermitian bands," Nature **598**(7879), 59–64 (2021).
24. A. Dutt, M. Minkov, I. A. D. Williamson, and S. Fan, "Higher-order topological insulators in synthetic dimensions," Light: Sci. Appl. **9**(1), 131 (2020).
25. W. Zhang and X. Zhang, "Quadrupole topological phases in the zero-dimensional optical cavity," Europhys. Lett. **131**(2), 24004 (2020).
26. Y. Hu, C. Reimer, A. Shams-Ansari, M. Zhang, and M. Loncar, "Realization of high-dimensional frequency crystals in electro-optic microcombs," Optica **7**(9), 1189–1194 (2020).
27. A. Balčytis, T. Ozawa, Y. Ota, S. Iwamoto, J. Maeda, and T. Baba, "Synthetic dimension band structures on a Si CMOS photonic platform," Sci. Adv. **8**(4), eabk0468 (2022).
28. C. Qin, F. Zhou, Y. Peng, D. Sounas, X. Zhu, B. Wang, J. Dong, X. Zhang, A. Alù, and P. Lu, "Spectrum control through discrete frequency diffraction in the presence of photonic gauge potentials," Phys. Rev. Lett. **120**(13), 133901 (2018).
29. M. C. Rechtsman, J. M. Zeuner, Y. Plotnik, Y. Lumer, D. Podolsky, F. Dreisow, S. Nolte, M. Segev, and A. Szameit, "Photonic Floquet topological insulators," Nature **496**(7444), 196–200 (2013).

Optics EXPRESS

30. M. Zhang, C. Wang, R. Cheng, A. Shams-Ansari, and M. Lončar, "Monolithic ultra-high-Q lithium niobate microring resonator," Optica **4**(12), 1536–1537 (2017).
31. C. Wang, M. Zhang, X. Chen, M. Bertrand, A. Shams-Ansari, S. Chandrasekhar, P. Winzer, and M. Lončar, "Integrated lithium niobate electro-optic modulators operating at CMOS-compatible voltages," Nature **562**(7725), 101–104 (2018).
32. M. Zhang, C. Wang, Y. Hu, A. Shams-Ansari, T. Ren, S. Fan, and M. Lončar, "Electronically programmable photonic molecule," Nat. Photonics **13**(1), 36–40 (2019).
33. C. Wang, M. Zhang, M. Yu, R. Zhu, H. Hu, and M. Loncar, "Monolithic lithium niobate photonic circuits for Kerr frequency comb generation and modulation," Nat. Commun. **10**(1), 978 (2019).
34. Y. Qi and Y. Li, "Integrated lithium niobate photonics," Nanophotonics **9**(6), 1287–1320 (2020).
35. D. Sun, Y. Zhang, D. Wang, W. Song, X. Liu, J. Pang, D. Geng, Y. Sang, and H. Liu, "Microstructure and domain engineering of lithium niobate crystal films for integrated photonic applications," Light: Sci. Appl. **9**(1), 197 (2020).
36. J. Zhou, Y. Liang, Z. Liu, W. Chu, H. Zhang, D. Yin, Z. Fang, R. Wu, J. Zhang, W. Chen, Z. Wang, Y. Zhou, M. Wang, and Y. Cheng, "On-chip integrated waveguide amplifiers on erbium-doped thin-film lithium niobate on insulator," Laser Photonics Rev. **15**(8), 2100030 (2021).
37. Y. Okawachi, M. Yu, B. Desiatov, B. Y. Kim, T. Hansson, M. Lončar, and A. L. Gaeta, "Chip-based self-referencing using integrated lithium niobate waveguides," Optica **7**(6), 702–707 (2020).
38. L. Cai, R. Kong, Y. Wang, and H. Hu, "Channel waveguides and y-junctions in x-cut single-crystal lithium niobate thin film," Opt. Express **23**(22), 29211–29221 (2015).
39. F. Thiele, F. v. Bruch, V. Quiring, R. Ricken, H. Herrmann, C. Eigner, C. Silberhorn, and T. J. Bartley, "Cryogenic electro-optic polarisation conversion in titanium in-diffused lithium niobate waveguides," Opt. Express **28**(20), 28961–28968 (2020).
40. L. Chang, Y. Li, N. Volet, L. Wang, J. Peters, and J. E. Bowers, "Thin film wavelength converters for photonic integrated circuits," Optica **3**(5), 531–535 (2016).
41. Z. Yu, Y. Tong, H. K. Tsang, and X. Sun, "High-dimensional communication on etchless lithium niobate platform with photonic bound states in the continuum," Nat. Commun. **11**(1), 2602 (2020).
42. J. Zhao, M. Rüsing, U. A. Javid, J. Ling, M. Li, Q. Lin, and S. Mookherjea, "Shallow-etched thin-film lithium niobate waveguides for highly-efficient second-harmonic generation," Opt. Express **28**(13), 19669–19682 (2020).
43. G. Li, D. Yu, L. Yuan, and X. Chen, "Single pulse manipulations in synthetic time-frequency space," Laser Photonics Rev. **16**(1), 2100340 (2022).
44. C. Qin, B. Wang, and P. Lu, "Frequency diffraction management through arbitrary engineering of photonic band structures," Opt. Express **26**(20), 25721–25735 (2018).
45. H. Lira, Z. Yu, S. Fan, and M. Lipson, "Electrically driven nonreciprocity induced by interband photonic transition on a silicon chip," Phys. Rev. Lett. **109**(3), 033901 (2012).
46. M. J. Zheng, J. J. Xiao, and K. W. Yu, "Controllable optical Bloch oscillation in planar graded optical waveguide arrays," Phys. Rev. A **81**(3), 033829 (2010).
47. W. P. Su, J. R. Schrieffer, and A. J. Heeger, "Soliton excitations in polyacetylene," Phys. Rev. B **22**(4), 2099–2111 (1980).
48. A. J. Heeger, S. Kivelson, J. R. Schrieffer, and W.-P. Su, "Solitons in conducting polymers," Rev. Mod. Phys. **60**(3), 781–850 (1988).
49. M. Atala, M. Aidelsburger, J. T. Barreiro, D. Abanin, T. Kitagawa, E. Demler, and I. Bloch, "Direct measurement of the Zak phase in topological Bloch bands," Nat. Phys. **9**(12), 795–800 (2013).
50. P. St-Jean, V. Goblot, E. Galopin, A. Lemaitre, T. Ozawa, L. Le Gratiet, I. Sagnes, J. Bloch, and A. Amo, "Lasing in topological edge states of a one-dimensional lattice," Nat. Photonics **11**(10), 651–656 (2017).
51. L. Zhang, Y. Yang, Z. Jiang, Q. Chen, Q. Yan, Z. Wu, B. Zhang, J. Huangfu, and H. Chen, "Demonstration of topological wireless power transfer," Sci. Bull. **66**(10), 974–980 (2021).
52. K. Fang, Z. Yu, and S. Fan, "Realizing effective magnetic field for photons by controlling the phase of dynamic modulation," Nat. Photonics **6**(11), 782–787 (2012).
53. D. R. Hofstadter, "Energy levels and wave functions of Bloch electrons in rational and irrational magnetic fields," Phys. Rev. B **14**(6), 2239–2249 (1976).
54. A. Celi, P. Massignan, J. Ruseckas, N. Goldman, I. B. Spielman, G. Juzeliūnas, and M. Lewenstein, "Synthetic gauge fields in synthetic dimensions," Phys. Rev. Lett. **112**(4), 043001 (2014).
55. M. Schmidt, S. Kessler, V. Peano, O. Painter, and F. Marquardt, "Optomechanical creation of magnetic fields for photons on a lattice," Optica **2**(7), 635–641 (2015).
56. R. Banerjee, T. C. H. Liew, and O. Kyriienko, "Realization of Hofstadter's buttefly and a one-way edge mode in a polaritonic system," Phys. Rev. B **98**(7), 075412 (2018).
57. L. Yuan, D. Wang, and S. Fan, "Synthetic gauge potential and effective magnetic field in a Raman medium undergoing molecular modulation," Phys. Rev. A **95**(3), 033801 (2017).
58. S. Fan, W. Suh, and J. D. Joannopoulos, "Temporal coupled-mode theory for the Fano resonance in optical resonators," J. Opt. Soc. Am. A **20**(3), 569–572 (2003).
59. W. Suh, Z. Wang, and S. Fan, "Temporal coupled-mode theory and the presence of non-orthogonal modes in lossless multimode cavities," IEEE J. Quantum Electron. **40**(10), 1511–1518 (2004).

Optics EXPRESS

60. L. Chang, M. H. P. Pfeiffer, N. Volet, M. Zervas, J. D. Peters, C. L. Manganelli, E. J. Stanton, Y. Li, T. J. Kippenberg, and J. E. Bowers, "Heterogeneous integration of lithium niobate and silicon nitride waveguides for wafer-scale photonic integrated circuits on silicon," Opt. Lett. **42**(4), 803–806 (2017).
61. M. He, M. Xu, Y. Ren, J. Jian, Z. Ruan, Y. Xu, S. Gao, S. Sun, X. Wen, L. Zhou, L. Liu, C. Guo, H. Chen, S. Yu, L. Liu, and X. Cai, "High-performance hybrid silicon and lithium niobate Mach-Zehnder modulators for 100 Gbit s^{-1} and beyond," Nat. Photonics **13**(5), 359–364 (2019).
62. X. Wang, P. O. Weigel, J. Zhao, M. Ruesing, and S. Mookherjea, "Achieving beyond-100-GHz large-signal modulation bandwidth in hybrid silicon photonics Mach Zehnder modulators using thin film lithium niobate," APL Photonics **4**(9), 096101 (2019).
63. Q. Shan, D. Yu, G. Li, L. Yuan, and X. Chen, "One-way topological states along vague boundaries in synthetic frequency dimensions including group velocity dispersion," Prog. Electromagn. Res. **169**, 33–43 (2020).
64. S. Longhi, "Dynamic localization and Bloch oscillations in the spectrum of a frequency mode-locked laser," Opt. Lett. **30**(7), 786–788 (2005).
65. M. Pan, H. Zhao, P. Miao, S. Longhi, and L. Feng, "Photonic zero mode in a non-Hermitian photonic lattice," Nat. Commun. **9**(1), 1308 (2018).
66. S. Xia, D. Kaltsas, D. Song, I. Komis, J. Xu, A. Szameit, H. Buljan, K. G. Makris, and Z. Chen, "Nonlinear tuning of PT symmetry and non-Hermitian topological states," Science **372**(6537), 72–76 (2021).
67. O. Zilberberg, S. Huang, J. Guglielmon, M. Wang, K. P. Chen, Y. E. Kraus, and M. C. Rechtsman, "Photonic topological boundary pumping as a probe of 4D quantum Hall physics," Nature **553**(7686), 59–62 (2018).
68. T. Cao, L. Fang, Y. Cao, N. Li, Z. Fan, and Z. Tao, "Dynamically reconfigurable topological edge state in phase change photonic crystals," Sci. Bull. **64**(12), 814–822 (2019).
69. A. Marandi, Z. Wang, K. Takata, R. L. Byer, and Y. Yamamoto, "Network of time-multiplexed optical parametric oscillators as a coherent Ising machine," Nat. Photonics **8**(12), 937–942 (2014).
70. H. Chalabi, S. Barik, S. Mittal, T. E. Murphy, M. Hafezi, and E. Waks, "Synthetic gauge field for two-dimensional time-multiplexed quantum random walks," Phys. Rev. Lett. **123**(15), 150503 (2019).
71. M. Aidelsburger, M. Atala, M. Lohse, J. T. Barreiro, B. Paredes, and I. Bloch, "Realization of the Hofstadter Hamiltonian with ultracold atoms in optical lattices," Phys. Rev. Lett. **111**(18), 185301 (2013).
72. M. Mancini, G. Pagano, G. Cappellini, L. Livi, M. Rider, J. Catani, C. Sias, P. Zoller, M. Inguscio, M. Dalmonte, and L. Fallani, "Observation of chiral edge states with neutral fermions in synthetic Hall ribbons," Science **349**(6255), 1510–1513 (2015).